

## Article

# Identification and Analysis of Low-Frequency Oscillation in a Multi-Grid-Forming-VSC Grid-Connected System

Min Zhang <sup>1</sup>, Rui Fan <sup>1</sup>, Huipeng Li <sup>1</sup>, Jun Zhao <sup>1</sup>, Tengxin Wang <sup>1</sup>  and Lin Chen <sup>2,\*</sup>

<sup>1</sup> State Grid Shanxi Electric Power Company Electric Power Research Institute, Taiyuan 030001, China; mevisan@126.com (M.Z.); frifzy@163.com (R.F.); huipeng\_li@163.com (H.L.); 18246153625@163.com (J.Z.); 15376150256@163.com (T.W.)

<sup>2</sup> School of Electrical and Electronic Engineering, North China Electric Power University, Beijing 102206, China

\* Correspondence: chen\_lin@ncepu.edu.cn

**Abstract:** The existing low-frequency oscillation analysis method of a multi-grid-forming-VSC (voltage source converter) is greatly affected by modeling accuracy, and its oscillation mode can only be determined by acquiring the control parameters of the system. Therefore, a method of identifying low-frequency oscillation characteristics of multi-VSC based on VMD (variational mode decomposition) and a Prony algorithm was proposed in this paper. The Prony algorithm is sensitive to noise, and its identification accuracy is greatly affected by noise. Thus, the VMD algorithm was utilized to denoise the measured data. Then, the Prony algorithm was applied to analyze the low-frequency oscillation of the measured data of single VSC and multi-VSC grid-connected systems, and its applicability to different grid-forming VSCs was verified. The error comparison results showed that the proposed low-frequency oscillation identification method had high accuracy. Furthermore, the influence of the number of parallel VSCs, grid strength and active output on the low-frequency oscillation of the system was investigated. Finally, the effectiveness of the proposed low-frequency oscillation method was verified by building a physical experimental platform.

**Keywords:** multi-VSC; Prony algorithm; low-frequency oscillation; VMD; identification



**Citation:** Zhang, M.; Fan, R.; Li, H.; Zhao, J.; Wang, T.; Chen, L.

Identification and Analysis of Low-Frequency Oscillation in a Multi-Grid-Forming-VSC Grid-Connected System. *Electronics* **2023**, *12*, 3740. <https://doi.org/10.3390/electronics12183740>

Academic Editors: Jizhong Zhu, Yun Liu, Lei Xi and Weiye Zheng

Received: 25 July 2023

Revised: 31 August 2023

Accepted: 1 September 2023

Published: 5 September 2023



**Copyright:** © 2023 by the authors. Licensee MDPI, Basel, Switzerland. This article is an open access article distributed under the terms and conditions of the Creative Commons Attribution (CC BY) license (<https://creativecommons.org/licenses/by/4.0/>).

## 1. Introduction

In order to cope with the environmental pressure caused by global warming, China has proposed the “double carbon” goal of achieving carbon peak in 2030 and carbon neutrality in 2060 [1,2], a situation where a high proportion of new energy sources and a high proportion of power electronics are connected. Large-scale development and utilization of renewable energy is an important technical means to achieve the goal of ‘double carbon’. With the integration of high-permeability new energy sources, the power system gradually presents a ‘double-high’ background [3,4], and new requirements are put forward for grid-forming-VSC, that is, multi-grid-forming-VSC are expected to have networking capabilities and inertial support capabilities [5]. The grid-forming VSC can directly determine the frequency of the node where it is located by controlling the phase angle of the output voltage, and exhibits voltage source characteristics to the grid, which has the advantages of off-grid/grouped-grid operation, weak-grid operation stability, and providing voltage support. The grid-connected VSC meets the needs of the “double high” background of the power grid, and the virtual synchronous generator (VSG) technology is a typical representative of the grid-forming VSC. Therefore, it has been rapidly developed [6].

At present, many scholars and experts have carried out extensive research on VSG, mainly focusing on the improvement of control strategy, cooperative operation, stability analysis, off/on grid mode switching, and so on [7,8]. However, the introduction of virtual inertia transforms the first-order characteristics of the active-frequency control loop into second-order oscillation characteristics [9]. Therefore, when VSG control is applied to microgrids, one problem that must be paid attention to is the low-frequency oscillation

introduced by the characteristics of the swing equation, which is an inherent characteristic of the synchronous generator (SG) and VSG [10].

Low-frequency oscillation is an important topic in traditional power system stability analysis. It refers to the relative swing between the rotors when the SG in parallel operation is disturbed, and the oscillation frequency of 0.1~2.5 Hz is generated on the transmission line due to insufficient system damping [11,12]. Because VSG provides the necessary moment of inertia, damping, frequency and voltage regulation support for the system by simulating the rotor motion equation of SG, the low-frequency oscillation caused by VSG is different from the low-frequency oscillation generated by the traditional system composed of SG: (1) The synchronous reactance of SG is inductive and large, which is related to its physical structure and magnetic circuit saturation. Therefore, the active power and reactive power of SG are decoupled, and its low-frequency oscillation characteristics are independent of reactive power. The output impedance of VSG is small, which is closely related to the underlying voltage control strategy and control parameters. Its active loop and reactive loop are coupled, so its low-frequency oscillation characteristics are affected by the reactive loop. (2) The rotational inertia, damping coefficient and magnetic field strength of SG are limited by the physical structure, while the rotational inertia, damping coefficient and electromagnetic parameters of VSG are relatively flexible and can be dynamically adjusted as needed, so the low-frequency oscillation frequency range generated by VSG is larger. (3) The dynamic characteristics of SG are generally in the low-frequency band, while the control bandwidth of VSG is higher, and its dynamic characteristics are distributed in a wider frequency band [10]. Therefore, the rapid monitoring of the new low-frequency oscillation characteristics generated by the power electronic converter connected to the system and the accurate identification of the low-frequency oscillation mode are helpful to realize the effective damping control of the power system and improve the stability of the power grid [13].

At present, there are two main identification methods for VSG low-frequency oscillation: one is the model analysis method, which analyzes the low-frequency oscillation characteristics of the system by constructing the physical model of the system [14]. This method is simple in calculation, but it needs to accurately obtain the control parameters of the system. When the system is in the gray box (black box), it cannot effectively identify the low-frequency oscillation characteristics of the system. In [15], the state space model of the multi-VSG parallel grid-connected system was constructed. The low-frequency oscillation characteristics of the system were studied by the eigenvalue analysis method, and the influence of different system parameters on the oscillation characteristics was analyzed. In [16,17], the admittance model of a multi-VSG parallel/grid-connected system was constructed, the transfer function expressions of VSG output power and angular frequency were derived, the applicable scope of the model was analyzed, and the influence of different system parameters on the low-frequency oscillation of the system was studied. The other is based on the measured data for identification, which can effectively avoid the influence of inaccurate physical models in the operation process, and can realize the online identification of low-frequency oscillation. Among them, the Prony algorithm is more widely used in the identification of low-frequency oscillations in conventional power systems. Aiming to address the problem of the Prony algorithm being sensitive to noise interference and difficult to identify the model order, it is easy to appear pseudo-mode. In [13], differential orthogonal matching pursuit and the Prony algorithm were proposed to identify the low-frequency oscillation modes of traditional power systems. In [18], the wavelet transform was used to filter out the noise of the measurement signal, and the singular value and total least squares method was used to improve the Prony algorithm, so as to realize the effective identification of multiple measurement signals. However, the above literature was devoted to the identification of low-frequency oscillation in traditional power systems. At present, there is no literature on the identification of low-frequency oscillation characteristics of grid-forming-VSC under the background of 'double high'.

Based on the analysis method of low-frequency oscillation in traditional power system, this paper proposed a method combining variational mode decomposition (VMD) and Prony algorithm to identify the low-frequency oscillation characteristics of grid-forming-VSC. Firstly, the VMD method was used to denoise the measurement data. Then, the Prony algorithm was used to analyze the low-frequency oscillation of the measurement data of single VSC and multi-VSC grid-connected systems, and its applicability to different VSCs was verified. On this basis, the variation law of low-frequency oscillation characteristics of the system was further studied when the number of parallel VSCs, the strength of the power grid and the active power output changed.

The paper is organized as follows. In Section 2, the extraction of modal signals based on the VMD algorithm is presented. Section 3 constructs a Prony identification model for low-frequency oscillations of a multiconfiguration mesh-type VSC, which includes three parts: parameter design, Prony identification process and model evaluation. The accuracy of the proposed Prony method is verified by simulation and experiment in Sections 4 and 5, respectively. Finally, Section 6 presents the conclusions.

## 2. Modal Signal Extraction Based on VMD Algorithm

Due to the existence of high-frequency stray components in the measured signal, the modal order identified by the Prony algorithm is often more than the dominant mode of the signal, and different degrees of noise will lead to inconsistent estimation order. Therefore, it is necessary to reduce the noise before using the Prony algorithm to analyze the low-frequency oscillation of the measured signal, so that the measured signal can approach the original signal to the maximum extent.

The VMD algorithm is a new adaptive signal decomposition method proposed by K. Dragomiretskiy et al. [19]. It solves the target mode by the intrinsic mode function [20]. It has the advantages of high accuracy and strong noise robustness. Therefore, this paper used the VMD algorithm to filter the noise of the VSC measurement signal. The specific process is as follows:

Assuming that the filtered signal is  $S(t)$  containing  $K$  modal functions  $u_k(t)$  ( $k = 1, 2, \dots, K$ ), the modal function  $u_k(t)$  is shown in Equation (1):

$$u_k(t) = A_k(t) \cos(\varphi(t)) \tag{1}$$

where the phase function  $\varphi_k(t)$  is an increasing function;  $A_k(t)$  is the instantaneous amplitude of  $u_k(t)$ ;  $\omega_k(t)$  is the instantaneous frequency.

$$\omega_k(t) = \frac{d\varphi(t)}{dx} \tag{2}$$

If  $A_k(t)$  and  $\omega_k(t)$  change slower than  $\varphi_k(t)$  in the time period  $[t - 2\pi/\omega_k(t), t + 2\pi/\omega_k(t)]$ , then  $u_k(t)$  is considered to be a harmonic signal with a frequency of  $\omega_k(t)$  and an amplitude of  $A_k(t)$ .

The Hilbert transform is used to decompose the filtered signal  $S(t)$ , and the unilateral spectrum of the modal function  $u_k(t)$  is solved:

$$\left[ \left( \delta(t) + \frac{j}{\pi t} \right) u_k(t) \right] e^{-j\omega_k(t)} \tag{3}$$

where  $\delta(t)$  denotes the unit impulse function.

By calculating the quadratic gradient, the original signal is decomposed into the set of intrinsic mode functions  $\{u_k\} = \{u_1, \dots, u_K\}$ . Then, the constrained variational problem is transformed into:

$$\begin{cases} \min_{\{u_k\}, \{\omega_k\}} \left\{ \sum_k \left\| \partial_t \left[ \left( \delta(t) + \frac{j}{\pi t} \right) u_k(t) \right] e^{-j\omega_k(t)} \right\|_2^2 \right\} \\ s.t. \quad \sum_k u_k(t) = S(t) \end{cases} \tag{4}$$

where  $\omega_k$  denotes the frequency center corresponding to the intrinsic mode  $u_k$ ;  $\partial_t$  denotes the partial derivative of  $t$ .

By introducing the quadratic penalty function term  $\alpha$  and the Lagrange multiplier  $\lambda(t)$ , the constrained variational problem of Equation (4) is transformed into the problem of solving the Lagrangian minimum, as shown below:

$$L(\{\omega_k\}, \{u_k\}, \lambda) = \alpha \sum_k \left\| \partial_t \left[ \left( \delta(t) + \frac{j}{\pi t} \right) u_k(t) \right] e^{-j\omega_k(t)} \right\|_2^2 + \left\| S(t) - \sum_k u_k(t) \right\|_2^2 + \langle \lambda(t), S(t) - \sum_k u_k(t) \rangle \quad (5)$$

In the presence of Gaussian noise,  $\alpha$  is used to guarantee the reconstruction accuracy of the signal, and  $\lambda(t)$  is used to guarantee the constraint condition. To solve the saddle point of the augmented Lagrange equation, the VMD method obtains the optimal solution of Equation (5) based on the alternating direction method of multiplication operator, so that the measured signal  $S(t)$  is decomposed into  $k$  intrinsic mode function components with limited bandwidth.

By using VMD to provide signal decomposition for the measured signal, the oscillation mode  $u_k(t)$  extracted by each VMD can be obtained. When the accuracy of VMD is high enough, for the  $n$ th extracted modal signal, there exists:

$$u_k(t) \approx S(t) \quad (6)$$

Based on VMD, all oscillation modal signals can be extracted from the original signal. After obtaining the  $u_k(t)$  of each modal signal obtained by VMD decomposition, the Prony algorithm can be used to effectively identify the low-frequency oscillation information of the measurement information [20].

Based on the above process, the noise reduction in the measurement signal can be completed, which lays a foundation for the subsequent identification using the Prony algorithm.

### 3. Prony Analysis

#### 3.1. Selection of Model Parameters

- (1) Sampling frequency: It can be seen from [4] that the oscillation frequencies of converters with different control strategies are quite different, and the low-frequency oscillation interval is larger than the traditional low-frequency oscillation interval of 0.1~2.5 Hz. Therefore, the sampling frequency needs to be determined by combining the maximum oscillation frequency of the converter and the sampling theorem. The excessive sampling frequency may lead to a poor fitting effect of the Prony algorithm.
- (2) Data length: It should contain at least two cycles of the lowest oscillation frequency, but not too long.
- (3) Model order  $p$ : Set the initial order of the model to  $p_e$ , so that it is much larger than the actual order, here take  $N/2$  [21] ( $N$  is the number of sampling points); then Prony analysis is performed on the simulation data to obtain  $p_e$  exponential components. The order  $p$  of the model for Prony analysis can be obtained by selecting the least  $p$  components from the  $p_e$  exponential components to make the square error satisfy the allowable error.

The selection of the above model parameters is not completely independent, and it needs to be further optimized in combination with the test in order to obtain a better fitting effect.

#### 3.2. Prony Algorithm

The Prony algorithm [22] is widely used in the study of low-frequency oscillation in traditional power systems. The basic principle is to use a linear combination of exponential functions to fit the system response, and then solve the frequency, attenuation factor, amplitude and phase of the corresponding signal.

Assume that the model of a measured signal  $x(0), x(1), \dots, x(n - 1)$  can be expressed as:

$$\hat{x}(n) = \sum_{m=1}^p b_m z_m^n \quad (n = 0, 1, \dots, N - 1) \tag{7}$$

$$\begin{cases} b_m = A_m \exp(j\theta_m) \\ z_m = \exp[(\alpha_m + j2\pi f_m)\Delta t] \end{cases} \tag{8}$$

$$\zeta_m = \frac{\alpha_m}{\sqrt{\alpha_m^2 + (2\pi f_m)^2}} \tag{9}$$

where  $A_m$  is amplitude;  $\theta_m$  is the initial phase;  $\alpha_m$  is the attenuation factor;  $f_m$  is the oscillation frequency,  $\zeta_m$  is the oscillation damping ratio;  $\Delta t$  is the sampling time interval,  $p$  is the fitting order and  $N$  is the number of sampling points.

The following will further introduce the solution steps of the Prony algorithm:

- (1) Define the following sample function:

$$r(i, j) = \sum_{n=p_e}^{N-1} x(n - j)x(n - i) \tag{10}$$

Based on Equation (10), the sample matrix shown in Equation (11) is obtained.

$$R = \begin{bmatrix} r(1, 0) & r(1, 1) & \dots & r(1, p_e) \\ r(2, 0) & r(2, 1) & \dots & r(2, p_e) \\ \vdots & \vdots & & \vdots \\ r(p_e, 0) & r(p_e, 1) & \dots & r(p_e, p_e) \end{bmatrix} \quad (p_e \gg p) \tag{11}$$

- (2) Using the total least squares method to determine the solution  $a_1, a_2, \dots, a_p$  of the linear prediction equation.

$$\begin{bmatrix} r(0, 0) & r(0, 1) & \dots & r(0, p) \\ r(1, 0) & r(1, 1) & \dots & r(1, p) \\ \vdots & \vdots & & \vdots \\ r(p, 0) & r(p, 1) & \dots & r(p, p) \end{bmatrix} \begin{bmatrix} 1 \\ a_1 \\ \vdots \\ a_p \end{bmatrix} = \begin{bmatrix} \varepsilon_p \\ 0 \\ \vdots \\ 0 \end{bmatrix} \tag{12}$$

- (3) Find the root  $z$  of polynomials in Equation (13).

$$1 + a_1 z^{-1} + \dots + a_p z^{-p} = 0 \tag{13}$$

- (4) Deduce  $\hat{x}(n)$  from Equation (14).

$$\hat{x}(n) = -\sum_{i=1}^p a_i \hat{x}(n - i), \quad \hat{x}(0) = x(0) \tag{14}$$

- (5) and then solve the matrix  $b$  according to Equation (15).

$$\begin{bmatrix} 1 & 1 & \dots & 1 \\ z_1 & z_2 & \dots & z_p \\ \vdots & \vdots & & \vdots \\ z_1^{N-1} & z_2^{N-1} & \dots & z_p^{N-1} \end{bmatrix} \begin{bmatrix} b_1 \\ b_2 \\ \vdots \\ b_p \end{bmatrix} = \begin{bmatrix} \hat{x}(0) \\ \hat{x}(1) \\ \vdots \\ \hat{x}(N - 1) \end{bmatrix} \tag{15}$$

- (6) The amplitude  $A_i$ , phase  $\theta_i$ , frequency  $f_i$  and attenuation factor  $\alpha_i$  are calculated by using Equation (16) to calculate the relevant parameters of the model.

$$\begin{cases} A_i = |b_i| \\ \theta_i = \arctan[\text{Im}(b_i)/\text{Re}(b_i)] \\ f_i = \arctan[\text{Im}(z_i)/\text{Re}(z_i)]/2\pi\Delta t \\ \alpha_i = \text{Im}|z_i|/\Delta t \end{cases} \quad (16)$$

### 3.3. Evaluation Indicators

In order to evaluate the fitting accuracy of the Prony algorithm, this paper measured the fitting effect of the Prony algorithm by calculating the square error of the measured data and the fitting data at different times. The calculation formula is as follows.

$$\text{Squared error} = (y(k) - \hat{y}(k))^2 \quad (17)$$

In summary, the specific process of Prony identification of low-frequency oscillation in VSC grid-connected system can be given, as shown in Figure 1.

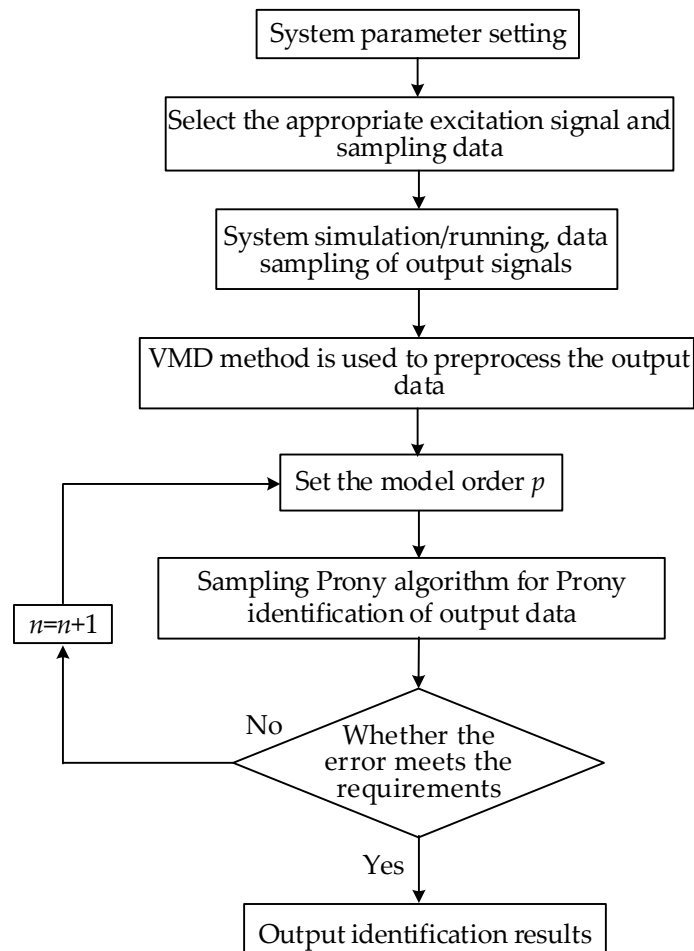


**Figure 1.** Flow chart of Prony method identification.

#### 4. Simulation Analysis

In order to verify the effectiveness of the low-frequency oscillation identification method proposed in this paper, a simulation model of six distributed generation (DG) grid-connected systems, shown in Figure 2, was built based on the simulation platform. The simulation parameters are shown in Table 1.

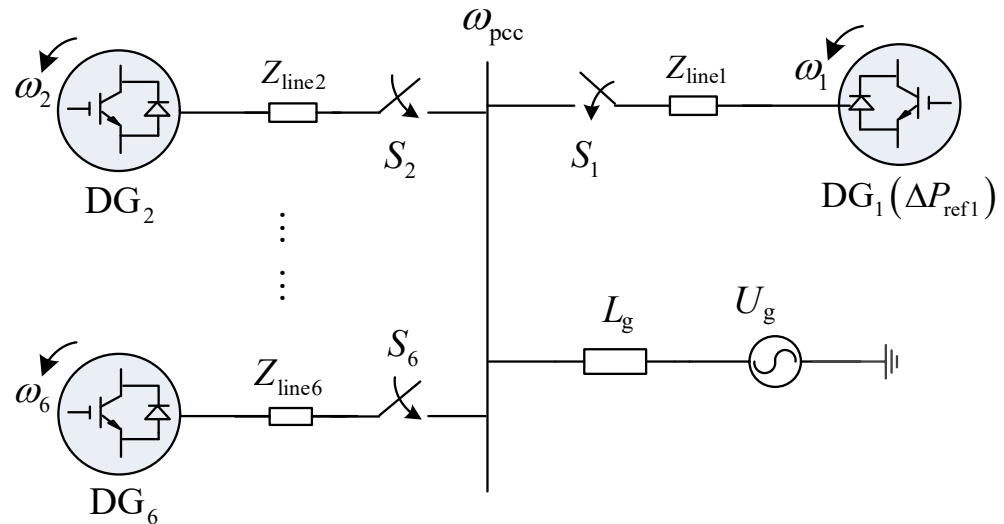


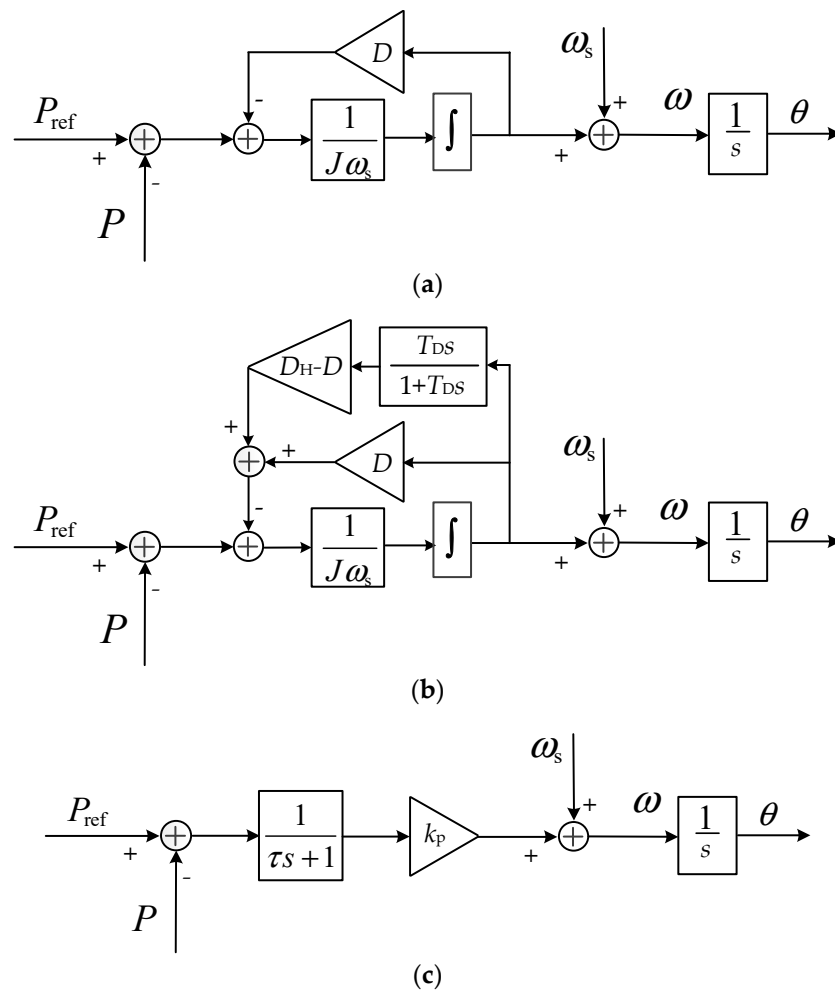
Figure 2. Structure diagram of simulation system.

Table 1. The parameters of the grid-connected inverter.

Parameter	Value
Capacity $S_N$	250 kVA
Grid frequency $f_g$	50 Hz
Grid impedance $L_g$	0.05 mH
Line impedance $Z_{line}$	0.0942 $\Omega$
Inertia coefficient $J$	5 kg·m <sup>2</sup>
Grid voltage $U_g$	380 V
DC voltage $U_{dc}$	800 V
Filter inductance $L_1$	0.3 mH
Filter capacitor $C$	68 $\mu$ F
Damping coefficient $D$	63.3 N·m·s·rad <sup>-1</sup>

The following three aspects will be studied:

- (1) Identification of low frequency oscillation characteristics of single VSC;
- (2) The low frequency oscillation identification of grid-forming-VSCs with different grid types. Among them, three typical grid-forming-VSC control schemes were selected: traditional VSG control scheme [16], improved VSG control scheme [23] and droop control scheme [4], as shown in Figure 3.
- (3) The influence of different system parameters on the characteristics of VSC low-frequency oscillation.



**Figure 3.** Active power-frequency control block diagram of VSC: (a) Traditional VSG control; (b) improved VSG control; (c) droop control.

4.1. Identification of Single VSC Low-Frequency Oscillation

Using the simulation model shown in Figure 2, DG<sub>1</sub> is controlled by VSG [16], and the system parameter information is shown in Table 1. The switch S<sub>1</sub> was closed, and it was a single VSC grid-connected mode. A 50 kW step disturbance was applied to the active power command P<sub>ref1</sub> of VSC<sub>1</sub> at 1 s. Figure 4 shows the comparison of VSC active power response curves before and after VMD denoising.

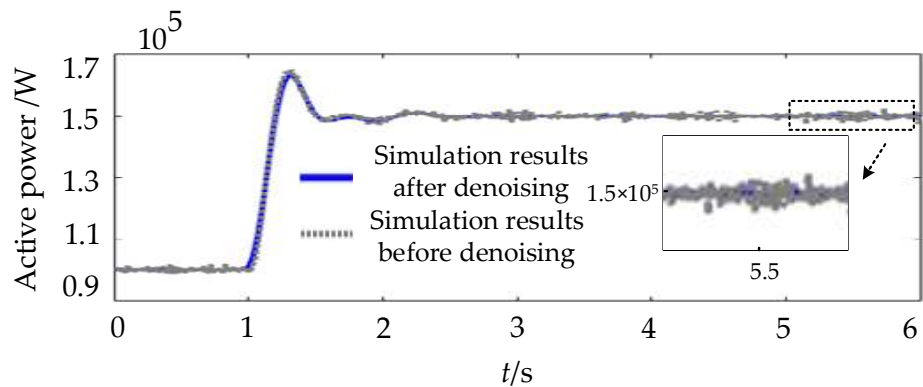


**Figure 4.** Active power response curve of VSC after and before VMD denoising.

It can be seen from Figure 4 that the VMD algorithm can effectively filter out the noise of VSC active power response. The active power response of VSC after filtering in Figure 5 is identified by Prony algorithm. The fitting results are shown in Figure 5, and the mean square error timing diagram is shown in Figure 6.

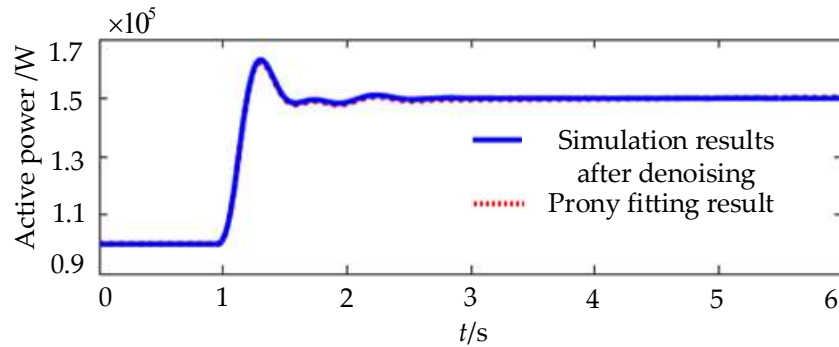


Figure 5. Fitting effect of Prony algorithm.

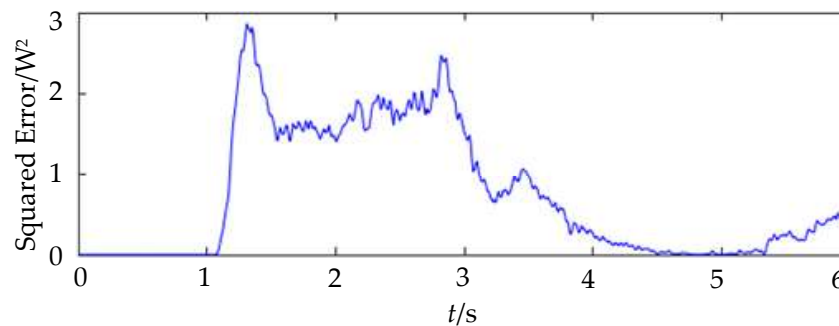


Figure 6. Fitting error timing diagram of Prony method.

It can be seen from Figures 5 and 6 that the Prony algorithm can better realize the fitting of VSC active power response, and the error was small. On this basis, the identification results and error comparison analysis results of Prony algorithm are given in Tables 2 and 3. Among them, the second row of Table 2 is the identification result without disturbance before 1 s, and the third row is the identification result with disturbance after 1 s.

Table 2. Prony identification results of single VSC.

$A_m$	$\alpha_m$	$f_m/\text{Hz}$	$\zeta_m$
$1.4 \times 10^6$	0.0013	0	1.05
$3.0 \times 10^5$	-2.12	3.21	0.105

Table 3. Comparative analysis of single VSC error results.

Identification Parameters		Prony Algorithm	VMD + Prony Algorithm
VSG control	$f_m/\text{Hz}$	3.35	3.21
	error/Hz	0.21	0.07
	$\zeta_m$	0.086	0.105
	error/%	12.7	4.6

The frequency and damping ratio of the oscillation mode were more concerned, and the error analysis of the two was carried out. From Tables 2 and 3, it can be seen that when the single VSC grid was disturbed, there was an oscillation mode in the system under the parameters set in this paper, and the oscillation frequency was about 3.21 Hz.

Compared with the direct Prony identification, the VMD algorithm was used to filter the VSC active power response, which can effectively improve the accuracy of Prony algorithm identification.

#### 4.2. Low-Frequency Oscillation Identification of Multi-VSC Grid-Connected System

Using the simulation model shown in Figure 2, the switches  $S_1$ ,  $S_2$  and  $S_3$  were closed in turn. At this time, the system was a three-machine parallel grid-connected mode. In order to verify the applicability of the proposed Prony identification method to other converter control strategies, the three typical grid-connected VSC control schemes shown in Figure 3 were selected for identification analysis. A 50 kW step disturbance was applied to the VSC active power command  $P_{ref1}$  controlled by VSG at 1 s. The active power response waveforms of the three control schemes are shown in Figure 7.

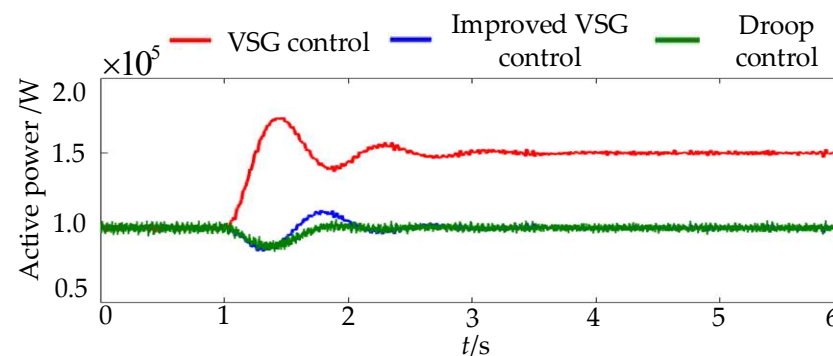


**Figure 7.** Active power response curves of different control schemes.

It can be seen from Figure 7 that under the disturbance of  $P_{ref1}$ , the three control schemes all produced the overshoot of active power, among which the VSG control and the improved VSG control produced the oscillation of active power. In addition, the output active power response noise of the three control schemes was large and needed to be filtered. The proposed Prony identification method was used to identify the low-frequency oscillation of the active power curve shown in Figure 7. The identification results are shown in Table 4. The results are shown in Table 4, the second line is the identification result without disturbance before 1 s, and the third to fifth lines are different VSC identification results with disturbance after 1 s. The results of the error comparison analysis are shown in Table 5.

From Tables 4 and 5, it can be seen that compared with the direct Prony algorithm identification, the accuracy of the frequency and damping ratio of the oscillation mode was higher after the VMD filtering and the Prony identification, and it had good applicability to grid-forming-VSC. When the multi-grid-forming-VSC was connected to the grid in parallel, there was an interaction between the active power response of the VSC under the disturbance of the active power command [16]. The low-frequency oscillation identification method proposed in this paper was used to analyze the active power waveform of the VSC output, which took into account the interaction between the loops. Therefore, the oscillation mode identification result was more accurate.

**Table 4.** Prony identification results of the multi-VSC system.

$A_m$	$\alpha_m$	$f_m/\text{Hz}$	$\zeta_m$
$1.4 \times 10^6$	$-6.6 \times 10^{-6}$	0	1.0
$3.7 \times 10^3$	-6.33	1.15	0.702
$3.0 \times 10^5$	-2.52	3.21	0.132
$2.9 \times 10^2$	-49	14.40	0.484

**Table 5.** Comparative analysis of identification errors of multi-VSC system.

Identification Parameters		Prony Algorithm	VMD + Prony Algorithm
VSG control	$f_m$ /Hz	1.23	1.15
	error/Hz	0.11	0.03
	$\xi_m$	0.752	0.702
	error/%	12.41	4.93
Improved VSG control	$f_m$ /Hz	3.52	3.21
	error/Hz	0.28	−0.03
	$\xi_m$	0.104	0.132
	error/%	15.4	7.32
Droop control	$f_m$ /Hz	13.03	14.40
	error/Hz	−1.05	0.32
	$\xi_m$	0.514	0.484
	error/%	9.36	2.98

#### 4.3. The Influence of Different Parameters on VSC Low-Frequency Oscillation

Based on the simulation model shown in Figure 2, the Prony algorithm was used to further study the influence of the number of parallel VSCs  $n$ , grid strength and VSC output on the low-frequency oscillation characteristics of the system. The grid strength is expressed by the short circuit ratio (SCR) [24]. The measurement data were collected when the number of parallel VSCs  $n$  were 2, 4 and 6, respectively. Subsequently, the number of parallel VSCs  $n = 4$  was set to further collect the measurement data when the SCR reflecting the grid strength was 14, 8 and 2 and the active power command step change  $\Delta P_{\text{ref}}$  of VSC<sub>1</sub> was 0.20 pu, 0.30 pu and 0.40 pu, respectively. Based on the process shown in Figure 1, Prony identification was performed on the collected measurement data, and the results are shown in Table 6.

**Table 6.** Prony analysis results under different parameters.

Parameter Information	$n = 2$	$n = 4$	$n = 6$	SCR = 14	SCR = 8	SCR = 2	$\Delta P_{\text{ref}} = 0.20$ pu	$\Delta P_{\text{ref}} = 0.30$ pu	$\Delta P_{\text{ref}} = 0.40$ pu
$f_m$ /Hz	0	0	0	0	0	0	0	0	0
$\alpha_m$	$3.5 \times 10^{-4}$	$1.1 \times 10^{-4}$	$2.4 \times 10^{-5}$	$-1.6 \times 10^{-4}$	$-1.0 \times 10^{-3}$	$-5.9 \times 10^{-3}$	$1.6 \times 10^{-3}$	$4.9 \times 10^{-4}$	$1.6 \times 10^{-3}$
$A_m$	$1.4 \times 10^6$	$1.4 \times 10^6$	$1.4 \times 10^6$	$1.4 \times 10^6$	$1.4 \times 10^6$	$1.4 \times 10^6$	$1.8 \times 10^6$	$2.3 \times 10^6$	$2.8 \times 10^6$
$\xi_m$	−1	−1	−1	1	1	1	−1	−1	−1
Modal 1									
$f_m$ /Hz	2.93	2.41	2.22	1.92	1.51	0.56	2.52	2.44	2.38
$\alpha_m$	−2.23	−2.28	−2.33	−2.31	−2.38	−2.89	−2.34	−2.52	−2.71
$A_m$	$1.5 \times 10^5$	$8.3 \times 10^4$	$5.6 \times 10^4$	$7.9 \times 10^4$	$7.6 \times 10^4$	$6.0 \times 10^4$	$1.2 \times 10^5$	$1.9 \times 10^5$	$2.6 \times 10^5$
$\xi_m$	0.120	0.149	0.165	0.189	0.247	0.635	0.146	0.162	0.178
Modal 2									
$f_m$ /Hz	3.6	3.6	3.5	3.5	3.5	3.5	3.6	3.6	3.6
$\alpha_m$	−2	−1.9	−1.9	−2	−2	−2	−1.9	−1.9	−1.8
$A_m$	$1.4 \times 10^5$	$2.2 \times 10^5$	$2.5 \times 10^5$	$2.2 \times 10^5$	$2.2 \times 10^5$	$2.2 \times 10^5$	$3.6 \times 10^5$	$5.3 \times 10^5$	$7.4 \times 10^5$
$\xi_m$	0.088	0.084	0.086	0.091	0.091	0.091	0.084	0.084	0.079

As can be seen from Table 6, the dominant mode oscillation frequencies were 1.92 Hz, 1.51 Hz and 0.56 Hz, while the damping ratios were 0.189, 0.247 and 0.635, respectively, using the analytical results of the Prony identification method proposed in this paper when the short-circuit ratio SCR was 14, 8 and 2, respectively. As the SCR decreased, the damping ratios gradually increased, and the low-frequency oscillation frequency moved to the low-frequency direction. In addition, there were two dominant oscillation modes in the system for different parameter variations. Among them, the oscillation frequency of mode 2 basically did not change with the change of parameters and remained around 3.6 Hz, and its damping ratio  $\xi$  also remained basically unchanged, indicating that this

oscillation mode was the inherent oscillation mode of the system. The oscillation frequency of mode 1 decreased gradually with the increase in the number of parallel VSCs and active output, and increased slightly with the enhancement of grid strength. In addition, the damping ratio  $\xi$  of mode 1 of the grid-connected system gradually increased when the number of parallel VSCs increased, the grid strength decreased and the active output increased, indicating that the risk of low-frequency oscillations of the system gradually decreased at this time.

### 5. Experimental Verification

In order to further verify the effectiveness of the proposed low-frequency oscillation identification method, an experimental platform of two VSG-controlled VSC grid-connected systems was built, as shown in Figure 8. The relevant experimental parameters are shown in Table 7.

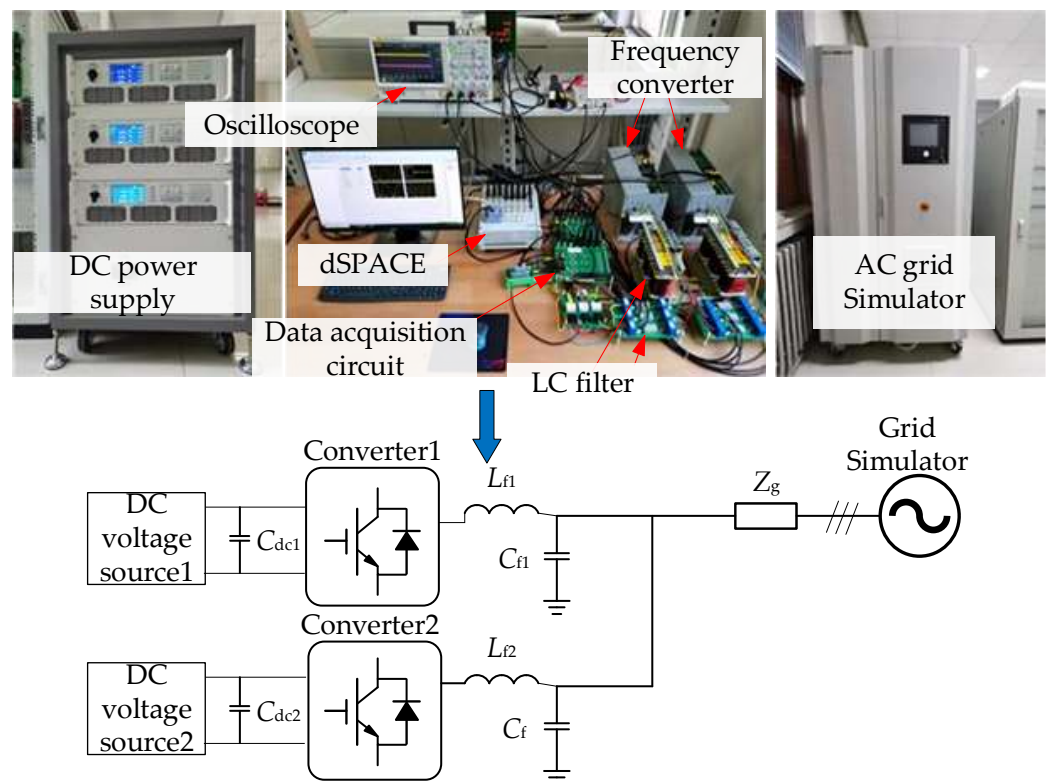
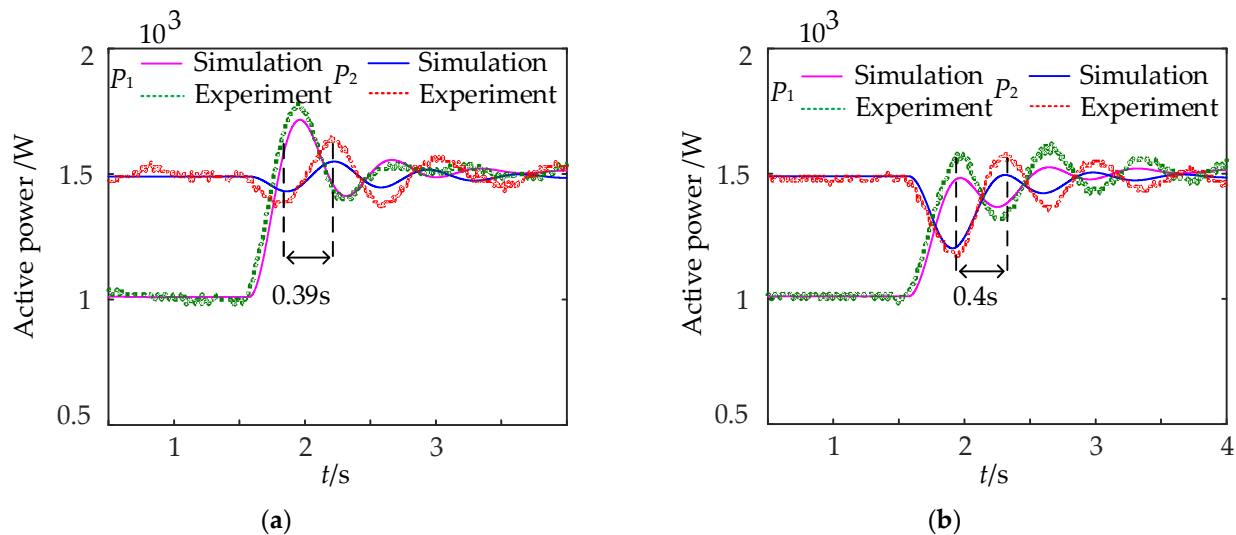


Figure 8. Experimental platform.

Table 7. Experiment parameters.

Parameter	Value
$S_N$ /kVA	2
$f$ /Hz	50
$L_g$ /mH	0.8
$R_g$ / $\Omega$	0.05
$J$ /kg·m <sup>2</sup>	0.81
$E_n$ /V	190
$V_{dc}$ /V	400
$L_{L1}$ /mH	4
$C_{C1}$ / $\mu$ F	10
$D$ /N·m·s·rad <sup>-1</sup>	6.08

The experimental conditions were set as follows: the initial active power command  $P_{ref1} = 1$  kW of VSC<sub>1</sub>,  $P_{ref2} = 1.5P_{ref1} = 1.5$  kW of VSC<sub>2</sub> and a step disturbance with an amplitude of 0.5 kW was applied to the active power command  $P_{ref1}$  of VSC<sub>1</sub> at 1 s. Figure 9 shows the experimental waveforms of the active power response of VSC under different SCR.



**Figure 9.** Experimental waveform of VSC step disturbance under different SCR: (a) SCR = 71.8; (b) SCR = 4.8.

It can be seen from Figure 9 that when a step disturbance was applied to the active power command of VSC<sub>1</sub>, the active power responses of VSC<sub>1</sub> and VSC<sub>2</sub> both produced severe low-frequency oscillation, indicating that there was a significant interaction between the power–frequency control loops of VSC. At the same time, it can be seen from Figure 9 that the active power oscillation trend of the experimental waveform was consistent with the simulation waveform, but there was a slight error between the two waveforms. Because the DC power supply and AC power grid in the simulation model were ideal models, the DC power supply (including the rectifier device) and AC power grid simulator were used in the experiment. In addition, due to the influence of VSC internal control delay and filtering, there was a slight error between the actual experimental results and the simulation results.

The Prony identification method proposed in this paper was used to identify the experimental results shown in Figure 9.

It can be known that when SCR = 71.8, the oscillation frequency  $f$  and damping ratio  $\zeta$  of the experimental waveform identified by the Prony method were 1.4 Hz and 0.089, respectively, and the oscillation frequency  $f$  and damping ratio  $\zeta$  of the simulated waveform were 1.5 Hz and 0.169, respectively. The reason for the large error between the two was that the DC power supply and the AC power grid simulator were used in the experiment. Among them, the DC power supply contained a rectifier device, and the ideal model was used in the simulation. When the strong network was changed into a weak network, the oscillation frequency of the VSC active power response waveform moved to the low-frequency direction and the damping ratio increased. The identification results of the simulation and experiment were consistent, which showed the effectiveness of the proposed Prony identification method. In addition, it is worth noting that when the grid strength became weak, the interaction between VSC control loops was enhanced.

## 6. Conclusions

In order to effectively identify the oscillation mode of the system when the system model is unknown, this paper proposed a Prony low-frequency oscillation identification method based on VMD. The main conclusions are as follows:

- (1) The Prony algorithm is sensitive to noise. The existence of noise will reduce the accuracy of the model. The VMD method is used to reduce the noise of the measured data, which can effectively improve the identification accuracy of the Prony algorithm. The consistency of simulation and experimental identification results further verified the accuracy and effectiveness of the proposed method.
- (2) The Prony algorithm does not need to model the system to be tested, and can effectively identify the low-frequency oscillation mode of the system only based on the measured data. It is not limited by the VSC control strategy and can be used for online identification of low-frequency oscillation. In addition, the low-frequency oscillation identification method takes into account the interaction between grid-connected VSCs, and the accuracy of the identification results is high.
- (3) There are two dominant oscillation modes in the system when different parameters change. Among them, the oscillation frequency and damping ratio of mode2 are basically unchanged, indicating that the oscillation mode is the inherent oscillation mode of the system. The oscillation frequency of mode1 decreases with the increase in  $n$  and  $\Delta P_{ref}$ , and increases with the increase in SCR. The damping ratio increases with the increase in  $n$  and  $\Delta P_{ref}$ , and decreases with the increase in SCR. The results showed that increasing  $n$  and  $\Delta P_{ref}$  and reducing SCR are helpful to reduce the risk of low-frequency oscillation of the system.

**Author Contributions:** Conceptualization, M.Z., R.F. and L.C.; methodology, M.Z. and L.C.; software, H.L. and J.Z.; validation, M.Z., T.W. and L.C.; formal analysis, R.F. and T.W.; investigation, M.Z. and R.F.; resources, R.F. and H.L.; data curation, J.Z. and L.C.; writing—original draft preparation, M.Z. and L.C.; writing—review and editing, M.Z. and L.C. All authors have read and agreed to the published version of the manuscript.

**Funding:** This research was funded by the State Grid Shanxi Electric Power Company Science and Technology Project Research (Research on the Key Technology of Modeling and Control of Generalized Power Impact Load Operation Characteristics Under Background of New Power Systems (52053022000A)).

**Institutional Review Board Statement:** Not applicable.

**Informed Consent Statement:** Not applicable.

**Data Availability Statement:** Not applicable.

**Acknowledgments:** We appreciate our reviewers and editors for their precious time.

**Conflicts of Interest:** The authors declare no conflict of interest.

## References

1. Guo, Z.; Wei, W.; Chen, L.; Dong, Z.; Mei, S. Impact of energy storage on renewable energy utilization: A geometric description. *IEEE Trans. Sustain. Energy* **2021**, *12*, 874–885. [\[CrossRef\]](#)
2. Hosseinzadeh, N.; Aziz, A.; Mahmud, A.; Gargoom, A.; Rabbani, M. Voltage stability of power systems with renewable-energy inverter-based generators: A Review. *Electronics* **2021**, *8*, 115. [\[CrossRef\]](#)
3. Fang, J.; Li, H.; Tang, Y.; Blaabjerg, F. On the inertia of future more-electronics power systems. *IEEE J. Emerg. Sel. Top. Power Electron.* **2019**, *7*, 2130–2146. [\[CrossRef\]](#)
4. Jia, J.; Yan, X.; Qin, B.; Zhang, B. Modeling and analysis of the torque-frequency dynamics for multi-VSC parallel system based on the equivalent admittance. *IEEE Trans. Power Deliv.* **2022**, *37*, 3597–3607. [\[CrossRef\]](#)
5. Roy, T.K.; Ghosh, S.K.; Saha, S. Robust backstepping global integral terminal sliding mode controller to enhance dynamic stability of hybrid AC/DC microgrids. *Pro. Control Mod. Power Syst.* **2023**, *8*, 8. [\[CrossRef\]](#)
6. Ali, K.S.; Masoud, K.G.; Mohammad, E. Grid-supporting inverters with improved dynamics using enhanced virtual synchronous machine (eVSM). *IEEE Trans. Ind. Electron.* **2019**, *66*, 3655–3667.
7. Li, D.; Zhu, Q.; Lin, S.; Bian, X.Y. A Self-Adaptive Inertia and Damping Combination Control of VSG to Support Frequency Stability. *IEEE Trans. Energy Convers.* **2017**, *32*, 397–398. [\[CrossRef\]](#)
8. Feng, K.; Liu, C. Distributed Hierarchical Control for Fast Frequency Restoration in VSG-Controlled Islanded Microgrids. *IEEE Open J. Ind. Electron. Soc.* **2022**, *3*, 496–506. [\[CrossRef\]](#)
9. Li, M.; Huang, W.; Tai, N.; Yang, L.; Duan, D.; Ma, Z. A dual-adaptivity inertia control strategy for virtual synchronous generator. *IEEE Trans. Power Syst.* **2020**, *35*, 594–604. [\[CrossRef\]](#)

10. Liu, J.; Miura, Y.; Ise, T. Comparison of dynamic characteristics between virtual synchronous generator and droop control in inverter-based distributed generators. *IEEE Trans. Power Electron.* **2016**, *31*, 3600–3611. [[CrossRef](#)]
11. Netto, M.; Mili, L. Robust data filtering for estimating electromechanical modes of oscillation via the multichannel prony method. *IEEE Trans. Power Syst.* **2018**, *33*, 4134–4143. [[CrossRef](#)]
12. Sun, L.; Zhao, X. Modelling and analysis of frequency-responsive wind turbine involved in power system ultra-low frequency oscillation. *IEEE Trans. Sustain. Energy* **2022**, *13*, 844–855. [[CrossRef](#)]
13. Zhang, A.Q.; Zhang, L.L.; Li, M.S.; Wu, Q.H. Identification of dominant low frequency oscillation modes based on blind source separation. *IEEE Trans. Power Syst.* **2017**, *32*, 4774–4782. [[CrossRef](#)]
14. Shen, C.; An, Z.; Dai, X.; Wei, W.; Ding, L. Measurement-based solution for low frequency oscillation analysis. *J. Mod. Power Syst. Clean Energy* **2016**, *4*, 406–413. [[CrossRef](#)]
15. Li, M.; Shu, S.; Wang, Y.; Yu, P.; Liu, Y.; Zhang, Z.; Hu, W.; Blaabjerg, F. Analysis and improvement of large-disturbance stability for grid-connected VSG based on output impedance optimization. *IEEE Trans. Power Electron.* **2022**, *37*, 9807–9826. [[CrossRef](#)]
16. Qin, B.; Xu, Y.; Yuan, C.; Jia, J. A Unified method of frequency oscillation characteristic analysis for multi-VSG grid-connected system. *IEEE Trans. Power Deliv.* **2022**, *37*, 279–289. [[CrossRef](#)]
17. Qin, B.; Xu, Y. Modal analysis of multi-VSG grid-connected power-frequency oscillation. *Proc. CSEE* **2021**, *41*, 6570–6581.
18. Ma, Y.; Zhao, S.; Liu, S. Online identification of low-frequency oscillations based on improved multi-signal prony algorithm. *Power Syst. Technol.* **2007**, *31*, 43–49.
19. Wang, Y.X.; Markert, R. Filter bank property of variational mode decomposition and its applications. *Signal Process.* **2016**, *120*, 509–521. [[CrossRef](#)]
20. Tang, J.; Zhu, J.; Li, Y. VMD based mode identification for broad-band oscillation in power system. *Power Syst. Prot. Control* **2019**, *47*, 1–8.
21. Grund, C.E.; Paserba, J.J.; Hauer, J.F.; Nilsson, S.L. Comparison of Prony and eigenanalysis for power system control design. *IEEE Trans. Power Syst.* **1993**, *8*, 964–971. [[CrossRef](#)]
22. Liu, S.; Zhao, S.; Yu, Z. Prony analysis of low frequency oscillation based on wavelet pretreatment technology. *Electric Power Autom. Equip.* **2007**, *27*, 64–67.
23. Yan, X.; Jia, J. Decoupling control of primary frequency regulation and rotational speed damping of VSG. *Power Syst. Technol.* **2019**, *43*, 1566–1575.
24. Liu, J.; Yao, W.; Wen, J. Small signal stability analysis and control of double-fed induction generator considering influence of PLL and power grid strength. *Proc. CSEE* **2017**, *37*, 3162–3173.

**Disclaimer/Publisher’s Note:** The statements, opinions and data contained in all publications are solely those of the individual author(s) and contributor(s) and not of MDPI and/or the editor(s). MDPI and/or the editor(s) disclaim responsibility for any injury to people or property resulting from any ideas, methods, instructions or products referred to in the content.